HHS Public Access

Author manuscript

Neuroimaging Clin N Am. Author manuscript; available in PMC 2018 November 01.

Published in final edited form as:

Neuroimaging Clin N Am. 2017 November ; 27(4): 621–633. doi:10.1016/j.nic.2017.06.011.

Resting state fMRI in Presurgical Functional Mapping: Sensorimotor Localization

Donna Dierker, MS[a], **Jarod L Roland, MD**[b], **Mudassar Kamran, MD**[a], **Jerrel Rutlin, BA**[a], **Carl D Hacker, MD, PhD**[d], **Daniel S Marcus, PhD**[a], **Mikhail Milchenko, PhD**[a], **Michelle M Miller-Thomas, MD**[a], **Tammie L Benzinger, MD, PhD**[a,b], **Abraham Z Snyder, MD, PhD**[a,c], **Eric C Leuthardt, MD**[a,d,*], and **Joshua S Shimony, MD, PhD**[a,*]

[a]Mallinckrodt Institute of Radiology

[b]Department of Neurological Surgery

[c]Department of Neurology

[d]Department of Biomedical Engineering

Synopsis

The goal of this article is to compare resting state fMRI with task fMRI as a tool for presurgical functional mapping of the sensorimotor (SM) region. Prior to tumor resection, 38 patients were scanned using both methods. The SM area was anatomically defined using two different software tools. Overlap of anatomical regions of interest with task activation maps and resting state networks was measured in the SM region. A paired t-test showed higher overlap between resting state maps and anatomical references as compared to task activation when using a maximal overlap criterion. Resting state derived maps are more comprehensive than those derived from task fMRI.

Keywords

Functional MRI (fMRI); Resting State fMRI (RS-fMRI); task fMRI (T-MRI); Resting State Networks (RSN); Multi-Layer Perceptron (MLP); Sensorimotor network (SMN)

Introduction

The first demonstration of correlated spontaneous fluctuations of the BOLD fMRI signal was reported in1995 by Biswal and colleagues [1]. This phenomenon currently is widely referred to as resting state functional connectivity [2,3]. The associated topographies are known as resting state networks (RSNs). Advances in our understanding of resting state

Corresponding Author: Joshua S Shimony: shimonyj@wustl.edu, Mallinckrodt Institute of Radiology, Campus Box 8131, Washington University School of Medicine, 4525 Scott Ave., Saint Louis, MO 63110 USA, Tel: 314-362-5949.

*Dr. Shimony and Dr. Leuthardt contributed equally to this work

functional connectivity and improved data processing techniques have enabled clinical application of resting state fMRI (RS-fMRI) for purposes of presurgical planning [4–16]. RS-fMRI is efficient and robust. Nevertheless, the predominant method for presurgical mapping of brain function currently remains task based fMRI (T-fMRI), using paradigms to "activate" the motor and language systems.

Several studies in normal cohorts have demonstrated that RSNs and T-fMRI responses exhibit similar, although not identical, topographies [17–19]. The primary advantage of functional mapping with RS-fMRI is that the patient is not required to comply with a task paradigm, although they must rest quietly in the scanner. RS-fMRI is compatible with light sedation and even sleep [20–24]. Thus, RS-fMRI is feasible in populations that are not candidates for T-fMRI, such as in young children and uncooperative or confused adults. Acquisition is simple and requires no specialized equipment or technical skills. For these reasons, use of RS-fMRI for presurgical mapping of function is increasing. It is therefore important to compare results obtained by these two methods to better understand their relative advantages and disadvantages.

Here, we compare and contrast the two methods from the technical perspective in a series of patients with brain tumors. We focus on the differences between the maps of the sensorimotor (SM) system as seen with T-fMRI versus RS-fMRI. We use the anatomic stability of the primary sensory and motor cortex within the precentral and postcentral gyri to compare fMRI with anatomic results, which cannot be done with the more variable language system. We also compare our results to similar literature in this area [25–28].

Methods

Patients

Patients were recruited from the Neurosurgery brain tumor service, initially as part of an NIH-funded tumor data base grant (CONDR NIH 5R01NS066905). All aspects of the study were approved by the Washington University (WU) Institutional Review Board. All patients provided informed consent. The following inclusion criteria were used: new diagnosis of primary brain tumor; age above 18 years; clinical need for an MRI scan including fMRI for presurgical planning as determined by the treating neurosurgeon. Additionally, we required that the patient had both a motor paradigm T-fMRI and a RS-fMRI scan. Exclusion criteria included: prior surgery for brain tumor, inability to have an MRI scan, or a patient referred from an outside institute with an MRI scan not performed at WU. Patient age, sex, and tumor characteristics are listed in Table 1.

Acquisition

Patients were scanned with either a Siemens 3T Trio or Skyra scanner (Erlangen, Germany) using a standard clinical presurgical tumor protocol. Anatomical imaging included T1-weighted (T1w) magnetization prepared rapid acquisition gradient echo (MPRAGE), T2-weighted (T2w) fast spin echo, FLAIR imaging, susceptibility-weighted imaging (SWI), pre- and post-contrast T1w fast spin echo in 3 projections. Specific sequences for presurgical

mapping included Diffusion Tensor imaging (DTI) for track tracing, T-fMRI for motor localization, and RS-fMRI.

Both the task and resting state fMRI was acquired using a T2* echo planar imaging (EPI) sequence (voxel size 3 × 3 × 3 mm; TE = 27 ms; TR = 2 s; field of view = 256 mm; flip angle = 90°). The motor task fMRI employed a block design in which finger tapping was repeated over 4 OFF/ON cycles, each OFF and ON block lasting for 20 s (10 frames) for a total of 80 frames (2:40 minutes total per T-fMRI run). For most subjects, only one motor task session was acquired. For eight subjects, a second motor task session was acquired, and for one subject, a third task session was acquired. Where more than one task session was usable, the session providing the maximum overlap index, as defined below, was used for the subsequent overlap analyses. RS-fMRI was always acquired as two 6-minute runs (total of 360 frames = 12 minutes).

Preprocessing

Resting State fMRI—Preprocessing of RS-fMRI data was performed using previously described techniques [29,30]. Preprocessing steps included compensation for slice dependent time shifts, elimination of systemic odd-even slice intensity differences due to interleaved acquisition, and rigid body correction for head movement within and across runs. Atlas transformation was achieved by composition of affine transforms connecting the fMRI volumes with the T2-weighted and MPRAGE structural images, resulting in a volumetric time series in $(3\ mm)^3$ atlas space. Additional preprocessing included: spatial smoothing (6 mm full width half maximum Gaussian blur in each direction), voxelwise removal of linear trends over each run, and temporal low pass filtering retaining frequencies <0.1 Hz. Spurious variance was reduced by regression of nuisance waveforms derived from head motion correction and extraction of the time series from regions of white matter and CSF. The whole brain (“global”) signal was included as a nuisance regressor [31,32]. Frame censoring was performed to minimize the impact of head motion on the correlation results [30]. Thus, frames (volumes) in which the root mean square (evaluated over the whole brain) change in voxel intensity relative to the previous frame exceeded 0.5% (relative to the whole brain mean) were excluded from the functional connectivity computations [33]. The preprocessed fMRI data then were analyzed by a previously trained multi-layer perceptron (MLP) [34]. The MLP assigns to each voxel 7 values expressing the likelihood of belonging to each of 7 RSNs. The sensori-motor network was defined as all voxels in which the MLP identified the SMN as the most likely RSN.

Task fMRI Processing—T-fMRI was processed as using standard general linear model methods. After preprocessing, activation maps were generated from the task fMRI as described in [35]. Activation maps were smoothed with a 7mm Gaussian filter and a subject-specific intracranial mask was applied. Both MLP SM maps and smoothed/masked activation maps were resampled to cubic 1mm for intersection with the high-resolution anatomical regions of interest (ROI) described below.

Anatomical Regions—We used two different methods for anatomically identifying the primary SM region. The Brodmann method is based on volumetric registration of each

individual to a standard atlas; this method is robust in the sense of working all cases but does not take into account individual sulcal anatomy. The FreeSurfer [36,37] method provides more accurate localization based on sulcal anatomy; however, the FreeSurfer method has a finite failure rate, especially when brain anatomy is distorted by tumor mass effect.

Brodmann Primary Sensory Motor (B-SM) ROI—The Brodmann SM anatomical ROI was projected to a volume ribbon 1.5mm above and below the Population Atlas Landmark Surface-based (PALS) mean mid-thickness atlas surface using Caret version 5.65 as shown in Figure 1 [38], then dilated to 10mm using Connectome Workbench (wb_command) [39].

FreeSurfer Primary Sensory Motor (FS-SM) ROI—The sensori-motor region was segmented using the patient's MPRAGE image through FreeSurfer (Version 5.3.0). Owing to concerns about tumors affecting stereotaxic registration and downstream processing, we input cubic 1mm MPRAGE images already in atlas space. We imported the FreeSurfer surfaces and volumes into Connectome Workbench (Version 1.2.3) using methods adapted from the Human Connectome Project [40]. Native mesh surfaces were used for visualization. All hemispheres were inspected to ensure quality control, using automatically generated Connectome Workbench scenes like those shown in Figure 2. This display addressed the accuracy of the Freesurfer segmentation and parcellation in SM cortex.

Where the quality of the segmentation was poor and/or the parcellation accuracy was doubtful (e.g., Supplementary Figure 1), the affected hemisphere was excluded from downstream analysis. No manual patching of the FreeSurfer results or other interventions were performed. The precentral and postcentral labels from the usable hemispheres were extracted from FreeSurfer's "aparc+aseg" output volume to compute the Jaccard index [41] overlap (see below).

Jaccard Index Overlap—To measure anatomical overlap we used the Jaccard index (*JI*) [41]. This index is sensitive to mismatch even when anatomical overlap is strong. For each subject, the anatomical ROI, thresholded task activation map, and thresholded MLP SMN were masked according to which hemispheres had valid anatomical ROIs. We define:

> A_{fMRI} = Area (number of non-zero voxels) in the thresholded T-fMRI or RS-fMRI image
>
> $Aanat$ = Area (number of non-zero voxels) in the anatomical ROI (Brodmann or FreeSurfer)

Then, the *JI* for either the task or MLP was computed as:

$$JI = \frac{\left(A_{fMRI} \cap A_{anat}\right)}{A_{fMRI} + A_{anat} - \left(A_{fMRI} \cap A_{anat}\right)},$$

where ∩ indicates the intersection operation. Two anatomical ROIs were used for this analysis, one minimizing subject exclusions and another more precisely addressing localization questions.

Task Threshold—To compute the overlap with the anatomical SM parcellation, we adapted methods similar to Sair et al. [16], choosing the task threshold with the maximum *JI* overlap with the anatomical ROI. We first zeroed out all negative activations and included zero voxels when computing the percentile, then iterated task threshold from 1 to 100 percentile. Iterating percentiles rather than incrementing the intensity directly was important for comparing between subjects with varied distributions of activation intensities.

MLP Threshold—The analysis was run two ways: First, the MLP threshold was fixed at 0.95, which has been used clinically in our institution for the last several years. Second, the MLP threshold was adjusted to maximize the *JI* in the anatomical ROI (FS-SM or B-SM), in the same manner as the task threshold.

Hemisphere Masks—To exclude hemispheres where the FS-SM ROIs were unreliable, hemisphere masks were applied to the volumes. These masks were also used for sub-analysis of unaffected-only overlaps, based on which hemisphere was affected.

Results

Four subjects were unable to complete the motor task. One subject was unable to complete any tasks, but completed RS-fMRI scanning. Another subject completed both task and RS-fMRI, but failed preprocessing for either task or RS-fMRI, owing to problems with atlas space registration. All of these subjects were excluded.

Eleven more subjects were excluded from the FS-SM analysis: Three failed to complete FreeSurfer processing (recon-all), and the remaining eight had problems with segmentation and labeling that rendered the FS-SM parcellation unreliable (e.g., Supplementary Figure 1). These subjects were included in the B-SM analyses. For 2 subjects, only the left hemisphere FS-SM was reliable; for 11 subjects, only the right hemisphere FS-SM was reliable. Masks were used to exclude the unreliable hemisphere's data. The B-SM is not subject-specific, but does allow more subjects to be included (e.g., fewer exclusions due to FreeSurfer processing/parcellation errors, most of which are tumor-related).

Fixed MLP Threshold

Table 2 lists paired t-tests between the *JI* of task and RS-fMRI. Overlap is greater for task in the B-SM, while overlap is greater for MLP in the FS-SM. The difference is significant in the FS-SM (both unaffected and all usable hemispheres).

Maximum JI MLP Threshold

Table 3 lists paired t-tests between the *JI* of task and RS-fMRI when the MLP threshold was set to the maximum *JI* within the ROI. In such cases, RS-fMRI overlap significantly exceeded the task except for affected hemispheres in the FS-SM. Only 14 of the affected hemispheres had usable FS-SM parcellations, compared to the 27 unaffected hemispheres.

Figure 3 shows surface representation examples of localization of the pre- and post-central gyri and central sulcus using maximum *JI* thresholds for both T-fMRI and RS-fMRI. Figure

3 illustrates examples of a low, medium, and high overlap. Ranks are based on the FS-SM analysis using all hemispheres passing FreeSurfer quality control inspection.

Figure 4 shows the corresponding volumetric/slice views for the same subjects and thresholds presented in Figure 3.

Discussion

Task fMRI currently is the predominant non-invasive method used for localization of eloquent cortex prior to neurosurgery. This technique is well established and available from most of the MR vendors. Successful T-fMRI mapping requires patient cooperation and depends on modest radiological expertise in acquiring and processing the data. Resting state fMRI is an alternative method of brain mapping, with substantial and growing support in the literature [4–16]. Several publications have demonstrated how RS-fMRI has been able to help individual patients in situations where T-fMRI was not available [11,42,43]. RS-fMRI does not require active patient participation (beyond laying still during the MRI scan) and data acquisition is simple [10,15]. However, analysis of the acquired data depends on substantial expertise. In our hands, RS-fMRI is more robust with a clinical failure rate of 13% as compared to 33% with T-fMRI. Here, we compare results obtained by the two methods with a focus on localization of the sensorimotor system, this being an area of primary concern for the surgeon.

Anatomical mapping of the SM system is facilitated by its consistency of anatomic localization to the pre- and post-central gyri. This consistency provides the opportunity to use anatomical localization as a reference to compare results obtained by both T-fMRI and RS-fMRI. We used two complementary methods of anatomical localization, one volumetric and atlas-based (less accurate but more robust), the other based on individually computed gyral segmentation (more accurate, but less robust).

Our comparison reflects the inherent differences between T-fMRI and RS-fMRI. Although both are based on fMRI, they measure different aspects of brain function. Task fMRI imposes a behavior on the subject and yields the representation of a fixed sensory, motor, or cognitive process. Resting state fMRI measures something very different; since there is no imposed task, RS-fMRI reveals resting state networks, that is, the topography of temporally synchronous spontaneous neural activity. Although the physiological functions of intrinsic brain activity remain uncertain (for discussion see [44,45]), RSNs are of practical interest as they topographically resemble fMRI responses to a wide range of cognitive, sensory, and motor tasks. Here, we compare T-fMRI responses to a finger-tapping task, which recruits the hand area of sensori-motor cortex, versus the full sensorimotor network as revealed by RS-fMRI, which is more extensive and includes Brodmann areas 1–4 as well as supplementary motor cortex.

In this context, the most informative comparison measure is reliability. Our selection of the full anatomical extent of the SM system is based on neurosurgical considerations. Estimating the full extent of the SM system delineates all areas that contribute to motor function, hence, should be preserved to reduce post-operative morbidity. Finger-tapping T-

fMRI provides a restricted estimate of the hand area, although this can be extrapolated to a more complete view of the SM system. That said, that extrapolation is subjective and potentially misleading. Especially, when some of the cortical areas of task activation are not purely motor in regards to cognitive operations (i.e. attention or sensory processes). Thus, we opted to make the comparison of the resting state data at two different thresholds, one at a maximal overlap criteria determined by the *JI*, and a second at a fixed threshold commonly used in our institution for pre-surgical planning. The RS-fMRI overlap index is significantly greater when using the maximal overlap criteria. The present results are more ambiguous with the fixed threshold, with T-fMRI showing a trend towards greater overlap when using the B-SM anatomy region, but RS-fMRI performing better when using the FS-SM anatomy reference. T-fMRI activates all regions of the brain recruited to perform a task (e.g., visual system), which is what it was designed to do, but not all regions are equally relevant in a given presurgical application. The MLP maps include secondary somatosensory cortex or S2, which shows responses to tactile stimulation [46]. Though this paper focused on the sensorimotor network, MLP also identifies visual, auditory/language, and other RSN's.

Interpretation of fMRI data is complicated by the question of potentially compromised neurovascular coupling [47], which has been reported to lead to false negative T-fMRI results in a high proportion of low-grade gliomas [48]. It has been suggested that altered RS-fMRI functional connectivity in the SM network can occur on the same basis in patients with brain tumors [49]. Although neurovascular uncoupling could be a contributor in the cases that fail our RS-fMRI analysis, our overall failure rate is low, and, in most cases, we can identify a specific cause for this failure, typically, patient motion or sedation. It is possible that neurovascular uncoupling is less of a problem in the current data set since we focused mostly on high-grade gliomas. Speculatively, MLP mapping is resistant to this phenomenon owing to its use of high quality prior information.

Several prior papers have compared task fMRI with resting state in the SM system. Mannfolk et al. [25] compared functional data in 10 healthy volunteers and focused primarily on within-session test-retest reliability. They conclude that both methods have comparable test-retest reliability. Additionally, they present comparable SM maps of the two methods side by side but do not report a numerical comparison. The resting state analysis was done using independent components analysis (ICA), since the authors correctly point out that placement of a seed could be difficult in a brain distorted by tumor mass effect. Although our RS-fMRI method uses prior information on the expected appearance of standard RSNs (entered into the neural network during the MLP training phase [34]) it is not a classical seed based approach. Nevertheless, the MLP has been shown to provide robust results even in brains distorted by tumors [50]. MLP RSN mapping is based not on the absolute location of a voxel (which can be shifted in a patient with a brain tumor) but on its connectivity pattern to the rest of the brain. This analytic design feature provides a robust prior [34].

Kristo et al. [26] also focused on test-retest reliability in 16 normal subjects, but across two scans spaced by 7 weeks. They report better overlap for the T-fMRI as compared to the resting state data, which had a "less focal spatial pattern", as would be expected from our preceding discussion. Importantly, they state: "…just like task fMRI, task-free fMRI can properly identify critical brain areas for motor task performance".

Rosazza et al. [27] compared T-fMRI vs. RS-fMRI in 13 patients with lesions close to the SM. They used a pre-processing schemes different from ours, and analyzed several tasks that included the hand, leg, and face areas. An additional novel aspect of their study was a comparison with intra-operative electro-cortical stimulation. The numerical criteria they used are not directly comparable to the present *JI*. We considered metrics like those used in Rosazza et al. [27] and Sair et al. [16], but ultimately chose to compare overlap of T-fMRI and RS-fMRI with a neutral anatomical ROI. Rosazza et al. report that RS-fMRI can localize the SM successfully, with partial agreement with T-fMRI and also describe larger areas of correlated activity defined with the RS-fMRI data. They conclude that, since the methods are not equivalent, RS-fMRI should not be an outright replacement for T-fMRI; however: “since there is significant agreement between the two techniques, RS-fMRI can be considered with caution as a potential alternative to T-MRI when patients are unable to perform the task”.

Hou et al. [28] compared the location of the hand motor functional areas as determined by RS-fMRI, T-fMRI, and anatomy in 10 healthy subjects and 25 patients with left hemisphere brain tumors. They determined that, for the majority of their tumor cases, there was too large of a discrepancy between the location of the hand motor area as determined by the T-fMRI, and the location as determined by the anatomy and RS-fMRI. Their conclusion was that RS-fMRI is an inadequate replacement for T-fMRI. We believe that the differences in methodology between our study and Hou et al. explain our discrepant conclusions. Hou et al. used a classic seed based approach in single subjects with a relatively small seed size. Although we have used a similar approach in the past, we no longer do so since the signal to noise ratio (SNR) is poor and can lead to erroneous results. Our current approach using the MLP overcomes limited SNR by using prior information obtained from a large sample of control subjects. Hou et al. also focused exclusively on the hand motor area whereas we focus on the full extent of the SM system.

When taken together and considered clinically, there are advantages to the RS-fMRI approach that go beyond the task-independent nature of the imaging acquisition. In this study, we found that RS-fMRI covered a larger portion of the sensorimotor system, rather than the more focal region identified with T-fMRI. From a neurosurgical standpoint, this is of high importance. Lesions that are to be resected can be in proximity to any portion of the motor system. In the case of task-based localization this either requires customized tasks to best assess motor location relevant to that lesion or if the same task is used consistently (i.e. finger tapping) requires the surgeon to extrapolate the area of activation to other areas presumed to be motor and thus introduces the potential for error. Having a more comprehensive representation is fundamentally better from a neurosurgical standpoint. Because of the unique anatomic nature of motor organization, a focal activation and associated anatomic extrapolations are still useable, but this does not hold true for other functional systems, such a language. As an example, a focal activation of language task does not necessarily identify the full language system, nor can those locations be anatomically inferred from the focal activations. Thus, while this study used the anatomic nature of motor systems as a “ground truth,” it highlights that resting state imaging approaches capture a more capacious assessment of the functional system. This has important implications for other functional systems where there are fewer anatomic cues for localization and where task will only provide a more restricted localization.

Conclusion

We compared localization of the SM system in 38 patients with brain tumors using finger tapping T-fMRI vs. RS-fMRI. Our reference comparison was anatomical information obtained from two different registration schemes. Since T-fMRI and RS-fMRI measure a different aspect of brain function (task activation vs. synchronous intrinsic activity) we did not expect identical results; However, as expected and in agreement with prior publications, both methods provided accurate representation of the SM region, with the resting state representation covering a larger portion of the SM system. We conclude that either method can provide the information necessary for appropriate pre-surgical planning, provided that the differences between the two methods are appropriately considered. Finally, we note RS-fMRI offers the logistical advantage of simple acquisition without the need for patient cooperation. However, effective RSN mapping requires considerable sophistication in both pre-processing of RS-fMRI data as well as in the application of advanced numerical techniques (i.e., MLP regression) to analyze the pre-processed data.

Acknowledgments

Acknowledgements and Disclosure of Funding:

Leuthardt: Christopher Davidson Brain Tumor Research Fund

Leuthardt, Shimony: NIH R01 CA203861

Benzinger, Marcus: Barnes-Jewish Hospital Foundation (800-88)

Dierker: Christopher Davidson Brain Tumor Research Fund

1P30NS09857701 NINDS Center Core for Brain Imaging

Roland: NIH R25NS090978-01

Shimony: NIH U54 HD087011 supported by the Eunice Kennedy Shriver National Institute Of Child Health & Human Development of the National Institutes of Health to the Intellectual and Developmental Disabilities Research Center at Washington University.

Marcus, Snyder: R01NS066905, P30NS048056, P30NS098577, R01 EB009352

Benzinger: NIA/NIH AG003991; 2UF1AG032438

References

1. Biswal B, Yetkin FZ, Haughton VM, Hyde JS. Functional connectivity in the motor cortex of resting human brain using echo-planar MRI. Magnetic resonance in medicine. Oct; 1995 34(4):537–541. [PubMed: 8524021]
2. Raichle ME. Two views of brain function. Trends Cogn Sci. Apr; 2010 14(4):180–190. [PubMed: 20206576]
3. Raichle ME. The restless brain: how intrinsic activity organizes brain function. Philos Trans R Soc Lond B Biol Sci. May 19.2015 370(1668):20140172. [PubMed: 25823869]
4. Kokkonen SM, Nikkinen J, Remes J, et al. Preoperative localization of the sensorimotor area using independent component analysis of resting-state fMRI. Magnetic resonance imaging. Jul; 2009 27(6):733–740. [PubMed: 19110394]
5. Shimony JS, Zhang D, Johnston JM, Fox MD, Roy A, Leuthardt EC. Resting-state spontaneous fluctuations in brain activity: a new paradigm for presurgical planning using fMRI. Academic radiology. May; 2009 16(5):578–583. [PubMed: 19345899]

6. Liu H, Buckner RL, Talukdar T, Tanaka N, Madsen JR, Stufflebeam SM. Task-free presurgical mapping using functional magnetic resonance imaging intrinsic activity. Journal of neurosurgery. Oct; 2009 111(4):746–754. [PubMed: 19361264]
7. Zhang D, Johnston JM, Fox MD, et al. Preoperative sensorimotor mapping in brain tumor patients using spontaneous fluctuations in neuronal activity imaged with functional magnetic resonance imaging: initial experience. Neurosurgery. Dec; 2009 65(6 Suppl):226–236. [PubMed: 19934999]
8. Bottger J, Margulies DS, Horn P, et al. A software tool for interactive exploration of intrinsic functional connectivity opens new perspectives for brain surgery. Acta neurochirurgica. Aug; 2011 153(8):1561–1572. [PubMed: 21461877]
9. Lee MH, Smyser CD, Shimony JS. Resting-state fMRI: a review of methods and clinical applications. AJNR. American journal of neuroradiology. Oct; 2013 34(10):1866–1872. [PubMed: 22936095]
10. Lang S, Duncan N, Northoff G. Resting-state functional magnetic resonance imaging: review of neurosurgical applications. Neurosurgery. May; 2014 74(5):453–464. discussion 464–455. [PubMed: 24492661]
11. Kamran M, Hacker CD, Allen MG, et al. Resting-state blood oxygen level-dependent functional magnetic resonance imaging for presurgical planning. Neuroimaging clinics of North America. Nov; 2014 24(4):655–669. [PubMed: 25441506]
12. Tie Y, Rigolo L, Norton IH, et al. Defining language networks from resting-state fMRI for surgical planning--a feasibility study. Human brain mapping. Mar; 2014 35(3):1018–1030. [PubMed: 23288627]
13. Leuthardt EC, Allen M, Kamran M, et al. Resting-State Blood Oxygen Level-Dependent Functional MRI: A Paradigm Shift in Preoperative Brain Mapping. Stereotactic and functional neurosurgery. 2015; 93(6):427–439. [PubMed: 26784290]
14. Hart MG, Price SJ, Suckling J. Functional connectivity networks for preoperative brain mapping in neurosurgery. Journal of neurosurgery. Aug 26.2016 :1–10.
15. Lee MH, Miller-Thomas MM, Benzinger TL, et al. Clinical Resting-state fMRI in the Preoperative Setting: Are We Ready for Prime Time? Topics in magnetic resonance imaging: TMRI. Feb; 2016 25(1):11–18. [PubMed: 26848556]
16. Sair HI, Yahyavi-Firouz-Abadi N, Calhoun VD, et al. Presurgical brain mapping of the language network in patients with brain tumors using resting-state fMRI: Comparison with task fMRI. Human brain mapping. Mar; 2016 37(3):913–923. [PubMed: 26663615]
17. Smith SM, Fox PT, Miller KL, et al. Correspondence of the brain's functional architecture during activation and rest. Proceedings of the National Academy of Sciences of the United States of America. Aug 04; 2009 106(31):13040–13045. [PubMed: 19620724]
18. Cordes D, Haughton VM, Arfanakis K, et al. Mapping functionally related regions of brain with functional connectivity MR imaging. AJNR. American journal of neuroradiology. Oct; 2000 21(9): 1636–1644. [PubMed: 11039342]
19. Yeo BT, Krienen FM, Eickhoff SB, et al. Functional Specialization and Flexibility in Human Association Cortex. Cereb Cortex. Oct; 2015 25(10):3654–3672. [PubMed: 25249407]
20. Larson-Prior LJ, Zempel JM, Nolan TS, Prior FW, Snyder AZ, Raichle ME. Cortical network functional connectivity in the descent to sleep. Proceedings of the National Academy of Sciences of the United States of America. Mar 17; 2009 106(11):4489–4494. [PubMed: 19255447]
21. Picchioni D, Pixa ML, Fukunaga M, et al. Decreased connectivity between the thalamus and the neocortex during human nonrapid eye movement sleep. Sleep. Feb; 2014 37(2):387–397. [PubMed: 24497667]
22. Samann PG, Wehrle R, Hoehn D, et al. Development of the brain's default mode network from wakefulness to slow wave sleep. Cereb Cortex. Sep; 2011 21(9):2082–2093. [PubMed: 21330468]
23. Tagliazucchi E, von Wegner F, Morzelewski A, Borisov S, Jahnke K, Laufs H. Automatic sleep staging using fMRI functional connectivity data. NeuroImage. Oct 15; 2012 63(1):63–72. [PubMed: 22743197]
24. Mhuircheartaigh RN, Rosenorn-Lanng D, Wise R, Jbabdi S, Rogers R, Tracey I. Cortical and subcortical connectivity changes during decreasing levels of consciousness in humans: a functional

magnetic resonance imaging study using propofol. The Journal of neuroscience: the official journal of the Society for Neuroscience. Jul 07; 2010 30(27):9095–9102. [PubMed: 20610743]

25. Mannfolk P, Nilsson M, Hansson H, et al. Can resting-state functional MRI serve as a complement to task-based mapping of sensorimotor function? A test-retest reliability study in healthy volunteers. Journal of magnetic resonance imaging: JMRI. Sep; 2011 34(3):511–517. [PubMed: 21761469]
26. Kristo G, Rutten GJ, Raemaekers M, de Gelder B, Rombouts SA, Ramsey NF. Task and task-free FMRI reproducibility comparison for motor network identification. Human brain mapping. Jan; 2014 35(1):340–352. [PubMed: 22987751]
27. Rosazza C, Aquino D, D'Incerti L, et al. Preoperative mapping of the sensorimotor cortex: comparative assessment of task-based and resting-state FMRI. PloS one. 2014; 9(6):e98860. [PubMed: 24914775]
28. Hou BL, Bhatia S, Carpenter JS. Quantitative comparisons on hand motor functional areas determined by resting state and task BOLD fMRI and anatomical MRI for pre-surgical planning of patients with brain tumors. NeuroImage. Clinical. 2016; 11:378–387. [PubMed: 27069871]
29. Brier MR, Thomas JB, Snyder AZ, et al. Loss of intranetwork and internetwork resting state functional connections with Alzheimer's disease progression. The Journal of neuroscience: the official journal of the Society for Neuroscience. Jun 27; 2012 32(26):8890–8899. [PubMed: 22745490]
30. Power JD, Mitra A, Laumann TO, Snyder AZ, Schlaggar BL, Petersen SE. Methods to detect, characterize, and remove motion artifact in resting state fMRI. NeuroImage. Jan 01.2014 84:320–341. [PubMed: 23994314]
31. Fox MD, Zhang D, Snyder AZ, Raichle ME. The global signal and observed anticorrelated resting state brain networks. Journal of neurophysiology. Jun; 2009 101(6):3270–3283. [PubMed: 19339462]
32. Power JD, Plitt M, Laumann TO, Martin A. Sources and implications of whole-brain fMRI signals in humans. NeuroImage. Feb 01.2017 146:609–625. [PubMed: 27751941]
33. Smyser CD, Inder TE, Shimony JS, et al. Longitudinal analysis of neural network development in preterm infants. Cereb Cortex. Dec; 2010 20(12):2852–2862. [PubMed: 20237243]
34. Hacker CD, Laumann TO, Szrama NP, et al. Resting state network estimation in individual subjects. NeuroImage. Nov 15.2013 82:616–633. [PubMed: 23735260]
35. Corbetta M, Kincade JM, Ollinger JM, McAvoy MP, Shulman GL. Voluntary orienting is dissociated from target detection in human posterior parietal cortex. Nature neuroscience. Mar; 2000 3(3):292–297. [PubMed: 10700263]
36. Dale AM, Fischl B, Sereno MI. Cortical surface-based analysis. I. Segmentation and surface reconstruction. NeuroImage. Feb; 1999 9(2):179–194. [PubMed: 9931268]
37. Desikan RS, Segonne F, Fischl B, et al. An automated labeling system for subdividing the human cerebral cortex on MRI scans into gyral based regions of interest. NeuroImage. Jul 01; 2006 31(3): 968–980. [PubMed: 16530430]
38. Van Essen DC. A Population-Average, Landmark- and Surface-based (PALS) atlas of human cerebral cortex. NeuroImage. Nov 15; 2005 28(3):635–662. [PubMed: 16172003]
39. Marcus DS, Harwell J, Olsen T, et al. Informatics and data mining tools and strategies for the human connectome project. Frontiers in neuroinformatics. 2011; 5:4. [PubMed: 21743807]
40. Van Essen DC, Smith SM, Barch DM, Behrens TE, Yacoub E, Ugurbil K. The WU-Minn Human Connectome Project: an overview. NeuroImage. Oct 15.2013 80:62–79. [PubMed: 23684880]
41. Jaccard P. The distribution of the flora in the alpine zone. New Phytologist. 1912; 11:37–50.
42. Batra P, Bandt SK, Leuthardt EC. Resting state functional connectivity magnetic resonance imaging integrated with intraoperative neuronavigation for functional mapping after aborted awake craniotomy. Surgical neurology international. 2016; 7:13. [PubMed: 26958419]
43. Roland JL, Hacker CD, Breshears JD, et al. Brain mapping in a patient with congenital blindness - a case for multimodal approaches. Frontiers in human neuroscience. 2013; 7:431. [PubMed: 23914170]
44. Laumann TO, Snyder AZ, Mitra A, et al. On the Stability of BOLD fMRI Correlations. Cereb Cortex. Sep 02.2016

45. Mitra A, Snyder AZ, Hacker CD, et al. Human cortical-hippocampal dialogue in wake and slow-wave sleep. Proceedings of the National Academy of Sciences of the United States of America. Nov 01; 2016 113(44):E6868–E6876. [PubMed: 27791089]

46. Burton H, Sinclair RJ, Wingert JR, Dierker DL. Multiple parietal operculum subdivisions in humans: tactile activation maps. Somatosensory & motor research. Sep; 2008 25(3):149–162. [PubMed: 18821280]

47. Agarwal S, Sair HI, Yahyavi-Firouz-Abadi N, Airan R, Pillai JJ. Neurovascular uncoupling in resting state fMRI demonstrated in patients with primary brain gliomas. Journal of magnetic resonance imaging: JMRI. Mar; 2016 43(3):620–626. [PubMed: 26201672]

48. Zaca D, Jovicich J, Nadar SR, Voyvodic JT, Pillai JJ. Cerebrovascular reactivity mapping in patients with low grade gliomas undergoing presurgical sensorimotor mapping with BOLD fMRI. Journal of magnetic resonance imaging: JMRI. Aug; 2014 40(2):383–390. [PubMed: 24338845]

49. Mallela AN, Peck KK, Petrovich-Brennan NM, Zhang Z, Lou W, Holodny AI. Altered Resting-State Functional Connectivity in the Hand Motor Network in Glioma Patients. Brain connectivity. Aug 22.2016

50. Mitchell TJ, Hacker CD, Breshears JD, et al. A novel data-driven approach to preoperative mapping of functional cortex using resting-state functional magnetic resonance imaging. Neurosurgery. Dec; 2013 73(6):969–982. discussion 982–963. [PubMed: 24264234]

Key Points

- Resting state fMRI data for mapping of functional systems is easy to acquire and does not require patient compliance.
- Resting state fMRI offers unique advantages and should be considered as a primary method in patients that are unable to comply with a task paradigm.
- Resting state derived maps are more extensive than those derived from task fMRI.
- Resting state fMRI can localize the sensorimotor cortex reliably and automatically.
- Neurosurgeons and neuroradiologists using task and resting fMRI should be aware of their respective advantages and disadvantages.

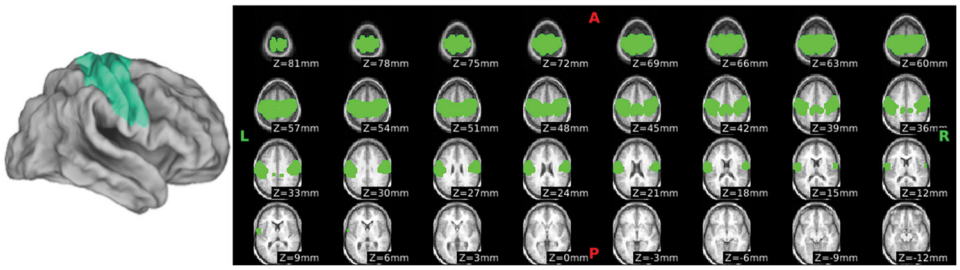

Figure 1.

Brodmann Primary SensoriMotor (B-SM) Anatomical Region of Interest (ROI)

Brodmann Areas 1, 2, 3, and 4 surface-based labels in the Population-Average, Landmark- and Surface-based (PALS) atlas were projected to a volume ribbon 1.5mm above and 1.5mm below the mean PALS midthickness surface in atlas space, and then dilated to a distance of 10mm. This ROI requires no exclusions, but does not precisely localize the subject's PSM.

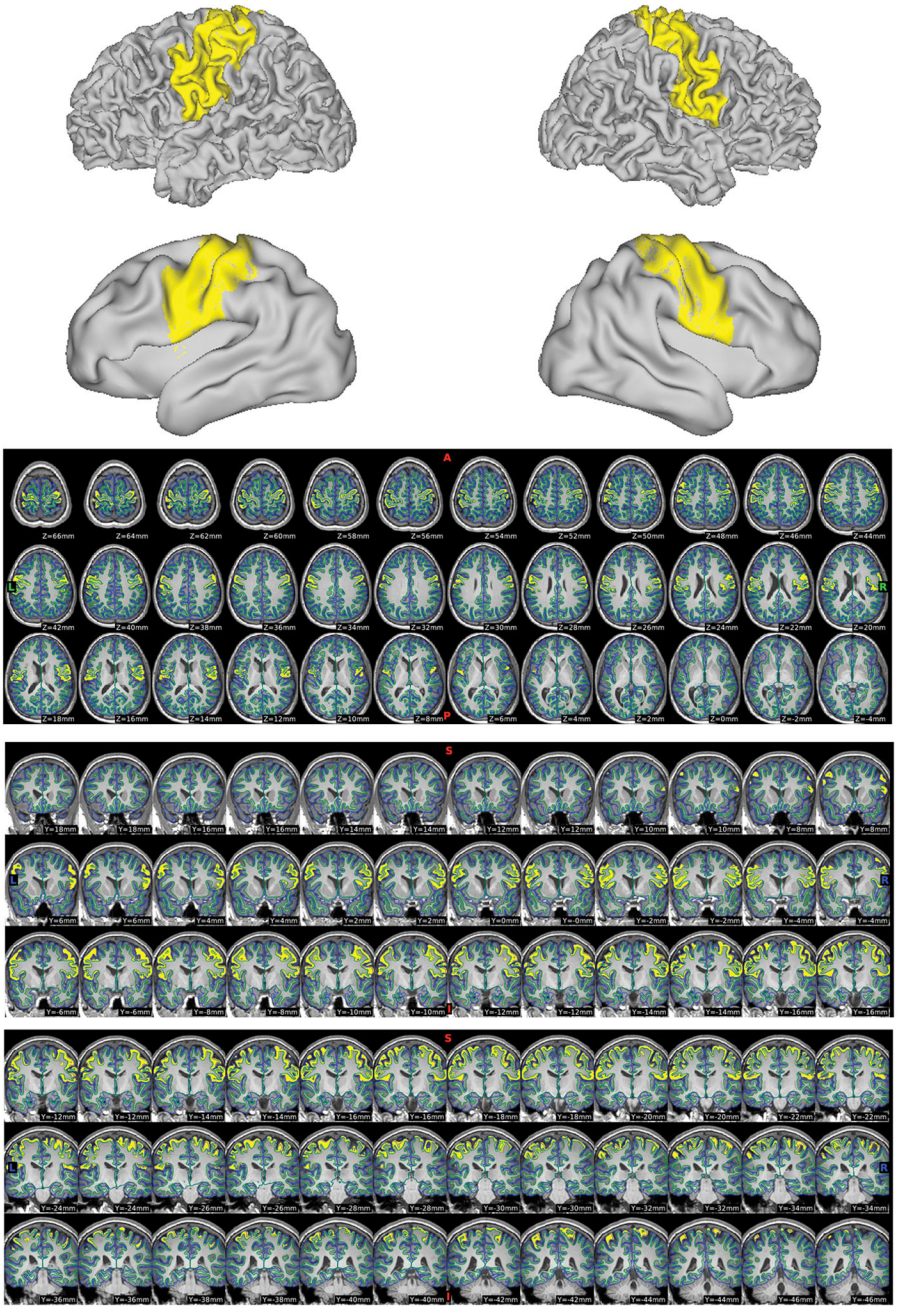

Figure 2.

Quality Control Scenes for FreeSurfer Pre-/Post-Central Parcels.

After creating template scenes, captures like this were generated for all subjects to determine which hemispheres had usable pre-/post-central parcellations for the overlap computations.

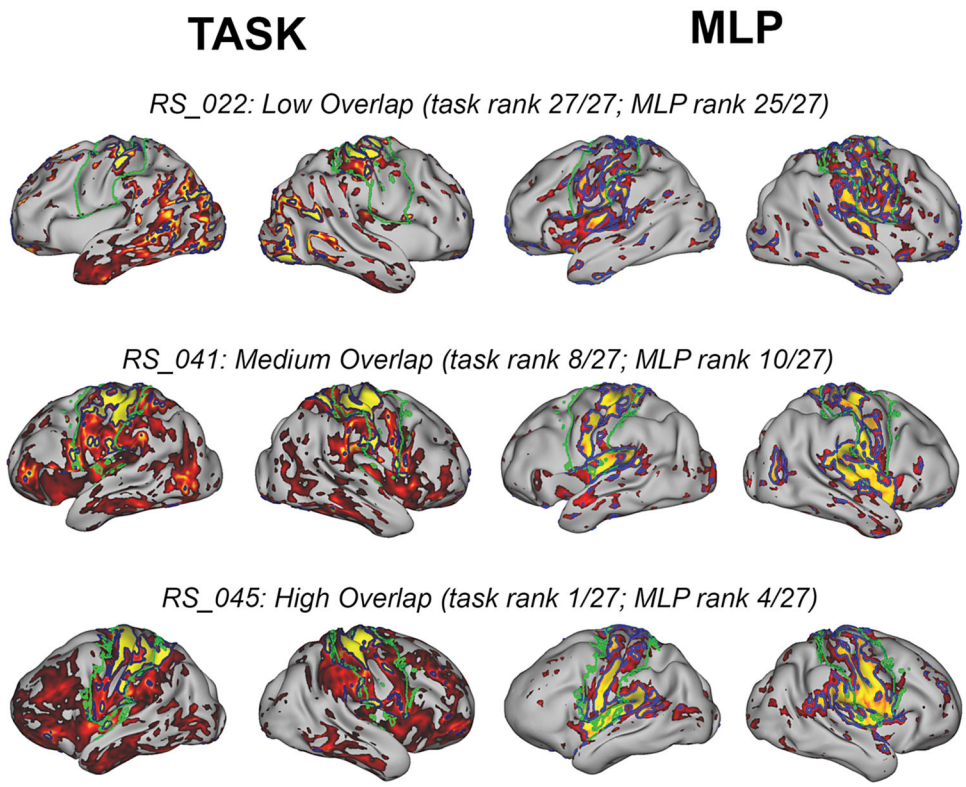

Figure 3.

Surface Views Across a Range of Jaccard Overlap Indices

Task activation maps (left) and MLP probability maps (right) are shown for subjects with low, medium, and high overlap with FS-SM on the patient's native mesh inflated surface. Green borders delimit FS-SM ROI (left and right columns). Task (left columns): Dark blue borders encircle regions exceeding the task threshold with maximum overlap. Task maps are scaled to 2.7, the mean of max overlap thresholds across subjects. MLP (right columns): Blue borders encircle regions exceeding the MLP threshold with maximum overlap. MLP probability maps are scaled 0.7 to 1.0.

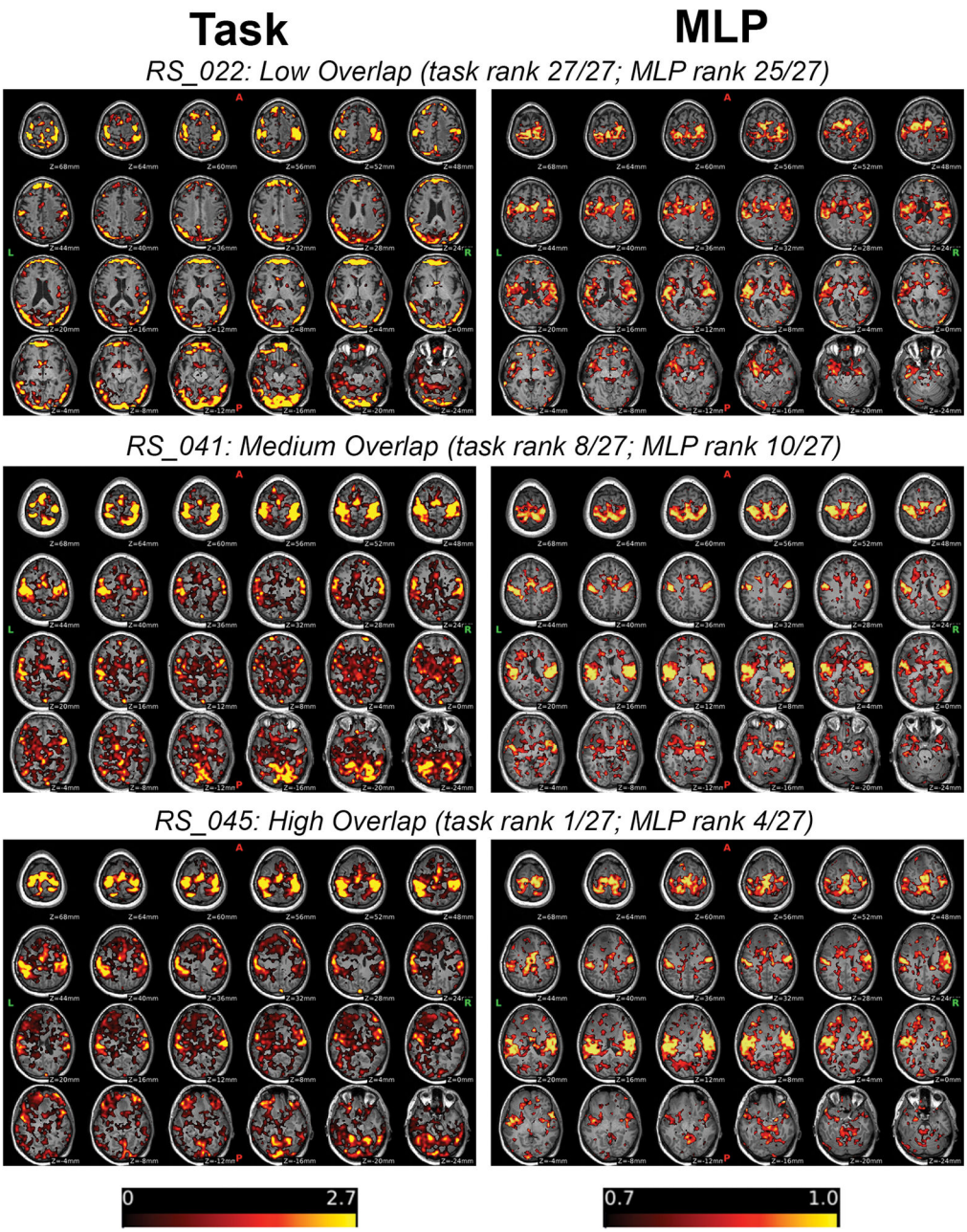

Figure 4.

Volume Views Across a Range of Overlap Indices

Top row: Task activation map (left) and MLP probability map (right) are shown for a patient with low FS-SM overlap laid over the patient's MPRAGE image. Task activation maps are scaled to 2.7, which is the mean maximum overlap threshold across subjects. MLP probability maps (right) are scaled 0.7 to 1.0. Corresponding views for subjects with medium and high overlap are also shown.

Table 1

Patient Clinical and Demographic Data

Patient ID	Age	Sex	Tumor Location	Tumor Size (ml)	Tumor Pathology
RS_001	31	M	Rght frontal lobe	70	Oligodendroglioma
RS_002	27	M	Left frontal lobe	11.7	Oligoastrocytoma
RS_003	44	M	Left basal ganglia	8.7	Glioblastoma
			Left temporal lobe	4.8	
RS_004	24	M	Left frontal lobe	56.2	Anaplastic glioma
RS_005	36	M	Left frontal lobe	1.2	Anaplastic mixed oligoastrocytoma
			Left frontal lobe	0.2	
RS_006	36	M	Left inferior frontal lobe	81.1	Anaplastic mixed oligoastrocytoma
RS_007	64	M	Left parieto-occipital	85.1	Glioblastoma,
RS_009	65	F	Left peritrigonal area	147	Glioblastoma
RS_010	50	F	Right peritrigonal area	15.5	Anaplastic astrocytoma
RS_011	24	M	Left frontotemporal	56.4	Mixed oligoastrocytoma
RS_012	42	M	Left frontal lobe	7.8	Anaplastic oligodendroglioma
RS_013	65	F	Right frontal lobe	8.5	Oligodendroglioma
RS_014	44	M	Left frontal/insular lobe	69.2	Oligodendroglioma
RS_015	62	F	Left frontal lobe	34.7	Mixed oligoastrocytoma
RS_016	57	F	Left insula	15.2	Glioblastoma
RS_017	54	M	Left frontal lobe	64.3	Mixed oligoastrocytoma
RS_018	39	F	Left frontal lobe	13.5	Oligodendroglioma
RS_019	33	F	Right frontoparietal	207	Anaplastic oliogdendroglioma
RS_021	25	M	Left frontal lobe	63.3	Mixed oligoastrocytoma
RS_022	67	M	Right frontal lobe	2.2	Metastatic lung carcinoma
RS_023	50	F	Left parietal/splenium	28.7	Oligodendroglioma
RS_024	56	M	Left frontal lobe	4.7	Anaplastic oligoastrocytoma
RS_028	64	M	Left parietal lobe	50.1	Glioblastoma
RS_029	52	M	Left frontal lobe	14.5	Oligodendroglioma
RS_030	71	M	Right BG/thalamus	16.6	Glioblastoma

Neuroimaging Clin N Am. Author manuscript; available in PMC 2018 November 01.

Patient ID	Age	Sex	Tumor Location	Tumor Size (ml)	Tumor Pathology
RS_031	53	F	Left thalamus	5.8	Glioblastoma
RS_032	46	M	Right temporal lobe	5.7	Glioblastoma
RS_033	37	M	Left frontal lobe	185	Mixed oligoastrocytoma
RS_035	28	F	Left temporal lobe	10.1	Oligoastrocytoma
RS_036	48	M	Left frontal lobe	20.6	Glioblastoma
RS_039	25	M	Right parietal lobe	32.0	Mixed oligoastrocytoma
RS_041	40	M	Left frontal lobe	23.3	Mixed oligoastrocytoma
RS_042	60	M	Left parietal lobe	0.7	Glioblastoma
RS_043	33	M	Right temporal lobe	4.0	Low-grade glioneuronal tumor
RS_044	23	M	Left frontal lobe	0.4	Ganglioglioma
RS_045	28	F	Both frontal lobes (left>right)	118	Anaplastic astrocytoma
RS_047	55	M	Left frontal lobe	66.2	Glioblastoma
RS_048	31	F	Right insula	14.3	Oligodendroglioma

Table 2

Paired t-test: Task vs RS-fMRI *JI* overlap by affected/unaffected and ROI: MLP thresholdFixed at 0.95 (* $p<0.05$)

Hemisphere/ROI	FS-SM anatomical ROI	B-SM anatomical ROI
All usable hemispheres	MLP>Task: p=0.0252* t=−2.376, n=27 mean-task=0.085 (stddev 0.038) mean-mlp=0.103 (stddev 0.039)	Task>MLP: p=0.1293 t=1.551, n=38 mean-task=0.162 (stddev 0.043) mean-mlp=0.144 (stddev 0.058)
Unaffected hemisphere only	MLP>Task: p=0.0027* t=−3.320, n=27 mean-task=0.082 (stddev 0.032) mean-mlp=0.106 (stddev 0.041)	Task>MLP: p=0.1261 t=1.565, n=38 mean-task=0.166 (stddev 0.048) mean-mlp=0.147 (stddev 0.062)
Affected hemisphere only	MLP>Task: p=0.2819 t=−1.123, n=14 mean-task=0.094 (stddev 0.049) mean-mlp=0.108 (stddev 0.038)	Task>MLP: p=0.1176 t=1.602, n=38 mean-task=0.160 (stddev 0.046) mean-mlp=0.140 (stddev 0.061)

Table 3

Paired t-test: Task vs. RS-fMRI *JI* overlap by affected/unaffected and ROI: MLP threshold maximizing *JI* (* p<0.05)

Hemisphere/ROI	FS-SM anatomical ROI	B-SM anatomical ROI
All usable hemispheres	MLP>Task: p=0.0037* t=−3.193, n=27 mean-task=0.085 (stddev 0.038) mean-mlp=0.109 (stddev 0.037)	MLP>Task: p<0.0001* t=−5.030, n=38 mean-task=0.162 (stddev 0.043) mean-mlp=0.219 (stddev 0.051)
Unaffected hemisphere only	MLP>Task: p=0.0004* t=−4.091, n=27 mean-task=0.082 (stddev 0.032) mean-mlp=0.110 (stddev 0.039)	MLP>Task: p=0.0001* t=−4.290, n=38 mean-task=0.166 (stddev 0.048) mean-mlp=0.220 (stddev 0.057)
Affected hemisphere only	MLP>Task: p=0.0924 t=−1.816, n=14 mean-task=0.094 (stddev 0.049) mean-mlp=0.115 (stddev 0.033)	MLP>Task: p<0.0001* t=−5.219, n=38 mean-task=0.160 (stddev 0.046) mean-mlp=0.220 (stddev 0.051)